[^{11}C]Flumazenil PET: Activity Images Versus Parametric Images for the Detection of Neocortical Epileptic Foci

Kaku Niimura, Otto Muzik, Diane C. Chugani, Chenggang Shen and Harry T. Chugani

Departments of Pediatrics, Neurology and Radiology, Children's Hospital of Michigan and Detroit Medical Center, Wayne State University School of Medicine, Detroit, Michigan

[^{11}C]flumazenil (FMZ) imaged with PET allows the computation of parametric images of both tracer influx (K1) and volume of distribution (VD). The VD images, which allow visualization of a quantitative measure of benzodiazepine receptor binding, are reported to have high sensitivity and specificity for the delineation of epileptic foci. However, the clinical feasibility of this method is compromised by the necessity of arterial blood sampling. We therefore compared the performance of parametric VD images against simple FMZ activity images for the detection of neocortical epileptic foci. **Methods:** FMZ PET data from 7 children with extratemporal lobe epilepsy (mean age [±SD] 9.8 ± 4.4 y) and 6 healthy adult volunteers (mean age [±SD] 40 ± 8 y) were analyzed using a semiautomated analysis algorithm. FMZ activity images and parametric VD images were analyzed for asymmetry with cutoff thresholds of 8%, 10% and 12%. **Results:** The time frame between 10 and 20 min after injection represented overall the best agreement between FMZ activity and VD images independent of the threshold. The normal asymmetry in VD images was determined as 6.4% ± 1.4% and was significantly higher in the FMZ activity images (7.6% ± 1.4%, $P = 0.001$). Increasing the cutoff threshold resulted in a significant decrease in the area defined as abnormal in both the VD and the FMZ activity images. Abnormalities defined in FMZ activity images identified additional brain regions as abnormal at the 8% threshold, but there was good agreement with VD images at the 10% asymmetry threshold. In those regions where abnormalities in VD and FMZ activity images were not matched, the asymmetry indices obtained from K1 images were significantly higher than those derived from the VD images ($P = 0.01$). **Conclusion:** Differences between VD and activity images above the 8% threshold are mainly due to K1. Abnormalities defined in FMZ activity images using a threshold of 10% agree well with those obtained from parametric VD images, indicating that activity images obtained from the time frame of 10–20 min are essentially equivalent to VD images with regard to detection of regions of abnormality for seizure focus localization.

Key Words: PET; epilepsy; flumazenil; benzodiazepine receptor; activity image; parametric image; volume of distribution

J Nucl Med 1999; 40:1985–1991

Received Nov. 24, 1998; revision accepted Apr. 19, 1999.

For correspondence or reprints contact: Otto Muzik, PhD, Department of Radiology/ PET Center, Children's Hospital of Michigan, 3901 Beaubien Blvd., Detroit, MI 48201.

The imaging of [^{11}C]flumazenil (FMZ) with PET has been shown to be a useful tracer for the study of benzodiazepine receptors (BZR) in vivo in humans with neurologic disorders (*1–3*). Reports by several investigators (*4–8*) indicate that abnormal BZR binding is a useful marker of epileptic foci in patients being evaluated for epilepsy surgery. Furthermore, FMZ PET has proven to be a more specific and sensitive method than fluorodeoxyglucose PET for visualization of both neocortical epileptic foci (*4,5*) and mesial temporal epileptic foci (*5–8*).

Quantification of FMZ images is performed most often using a two-compartment model introduced by Koeppe et al. (*9*). This model yields parametric images of the volume of distribution (VD) of the tracer in tissue (representing an index of BZR binding) and the ligand influx rate constant (K1). However, the computation of both VD and K1 requires the sampling of an arterial blood input function. Routine clinical application of this method for seizure foci detection in the pediatric population would be greatly facilitated if the protocol could be simplified by eliminating the need for arterial blood sampling and mathematic modeling.

To simplify the protocol and make it more feasible for clinical practice, our objective was to assess the agreement between the size and the location of abnormalities identified in simple FMZ activity images, against those defined in parametric VD images derived from a two-compartment model in patients with epilepsy. Our hypothesis was that, using an appropriate asymmetry threshold and time frame, FMZ activity images are as well suited as parametric VD images to identify foci of decreased BZR binding.

MATERIALS AND METHODS

Patients

The study population consisted of 7 children (5 boys, 2 girls; mean age [±SD] 9.8 ± 4.4 y) with neocortical epilepsy determined by seizure semiology or electroencephalography. None of the patients showed lesions on MR images. In addition, 6 healthy adults (4 men, 2 women; mean age [±SD] 40.0 ± 8.1 y) were recruited. All studies were performed in compliance with the Human Investigation Committee and the Radioactive Drug Research Committee at Wayne State University (Detroit, MI).

FMZ PET Procedures

FMZ PET studies were performed using the EXACT/HR (CTI/Siemens, Knoxville, TN) whole-body PET scanner at Children's Hospital of Michigan. This scanner has a 15-cm field of view and generates 47 image planes with a slice thickness of 3.125 mm. The reconstructed image in-plane resolution obtained was 5.5 ± 0.35 mm at full width at half maximum and 6.0 ± 0.49 mm in the axial direction (reconstruction parameters: Shepp-Logan filter with 1.0 cycle/cm cutoff frequency). A venous line was established for injection of FMZ (15 MBq/kg), and an arterial line was placed in a percutaneous radial artery for collection of 23 timed arterial blood samples (0.5 mL/sample, sequence: 12 × 10 s, 3 × 1 min, 2 × 2.5 min, 2 × 5 min, 4 × 10 min). Radioactivity in plasma was measured using a Cobra II gamma counter (Packard Instruments, Meriden, CT). FMZ and metabolites were determined using the method of Barre et al. (*10*). Beginning at the time of FMZ injection, a 60-min dynamic PET scan of the brain was obtained (sequence: 4 × 30 s, 3 × 1 min, 2 × 2.5 min, 2 × 5 min, 4 × 10 min). Electroencephalography was recorded for the duration of the study to ensure that scans were obtained in the interictal state.

Data Analysis

Compartmental analysis of dynamic PET and metabolite-corrected blood data was performed according to the method described by Koeppe et al. (*9*) to determine the VD and K1 parameters on a pixel-by-pixel basis. In addition, summed FMZ activity images of various lengths were obtained (time frames of 5–10, 10–20 and 15–30 min after injection). Regional abnormalities in both FMZ activity images and parametric VD images were identified using a semiautomated analysis algorithm (*11*), which allows operator-independent definition of abnormal cortical areas in transaxial images. The brain contour was determined automatically as a 25% isocontour, and an outline and concentric inner line were drawn by the program to define the thickness of the cortex. The data contained in this area (cortical region) were then divided into 60 regions per hemisphere, resulting in 60 cortical data values for each hemisphere. The data values for the left and right hemisphere were then displayed as cortical profiles. Subsequently, both profiles were overlaid so that the corresponding cortical values of both hemispheres could be found at the same ordinate. An asymmetry index was defined as:

$$[[H - L]/[L + H] \times 0.5] \times 100\%, \qquad \text{Eq. 1}$$

where L is the lower and H is the higher value, respectively. If the asymmetry between the corresponding cortical profile elements at a certain ordinate exceeded the cutoff threshold, the lower profile region was marked. Then, a new static "marked" image file was created that included all 47 planes of the original frame. A series of representative marked planes is shown in Figure 1. Finally, the marked image sets underwent three-dimensional maximal surface projection to display the marked regions with lower FMZ activity or BZR binding on the brain surface. On the basis of these processed views, the user outlined manually the marked regions, thus creating regions of interest (ROIs) in the FMZ activity images (ROI_{act}) and in the VD images (ROI_{VD}) (Fig. 2).

Study Design

It was shown previously that parametric VD images represent cortical BZR receptor abnormalities independent of blood flow (*9,12,13*). Initially, the normal asymmetry index observed in transverse VD image planes was derived from all supratentorial planes of the control subjects. We then chose cutoff thresholds of 1.0, 2.5 and 4.0 SD below this normal mean to represent cortical BZR binding abnormalities. Abnormal ROIs were then determined in the patient group in both the transverse VD and FMZ activity images, corresponding to the above cutoff thresholds. These abnormalities were marked with a value twice that found in the whole image volume, so that after applying a three-dimensional

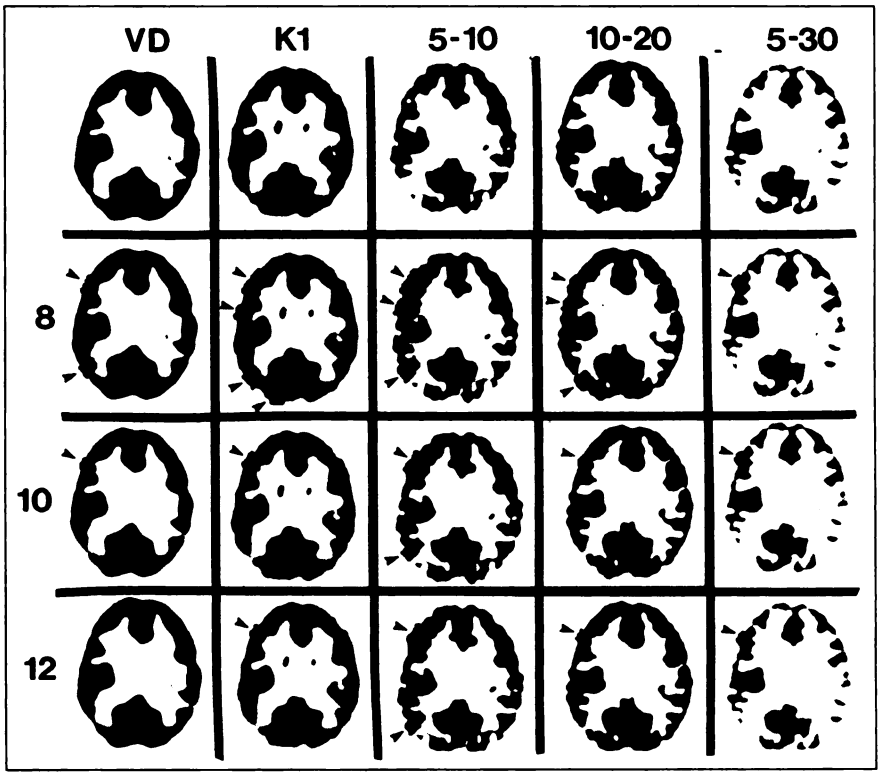

FIGURE 1. Transaxial images of (left to right) volume of distribution (VD), ligand influx rate constant (K1) and FMZ activity time frames of 5–10, 10–20 and 15–30 min (top row). Image planes were marked at 8% (second row), 10% (third row) and 12% (fourth row) cutoff thresholds. Marked cortical asymmetries are denoted by arrows.

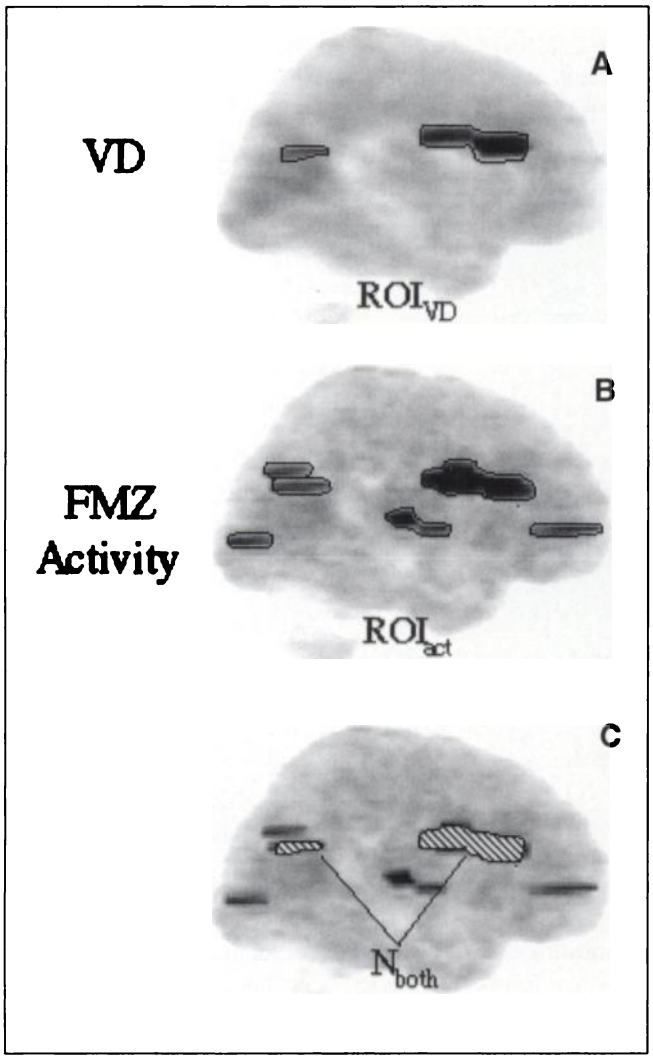

FIGURE 2. Three-dimensional projection images show marked regions of abnormalities in black. Regions of interest (ROIs, indicated by solid black lines) are defined in processed three-dimensional views of volume of distribution (VD) (ROI_{VD}, top) and [^{11}C]flumazenil (FMZ) activity image volumes (ROI_{act}, middle). ROIs were overlaid (bottom), and pixel number in ROI_{VD}, ROI_{act} and region common to ROI_{VD} and ROI_{act} (N_{both}, hatched region) were determined.

maximal surface projection, they could be displayed on the brain surface. In these newly created views, abnormal ROIs were defined manually in both the ROI_{VD} and the ROI_{act}. Subsequently, the ROI_{act} and ROI_{VD} were overlaid, and the number of image pixels common to both regions (N_{both}) or associated with only one or the other region (N_{act} and N_{VD}) was determined (Fig. 2). The agreement index between regions was defined as:

$$[N_{both}/N_{VD}] \times 100\%, \quad \text{Eq. 2}$$

indicating the percentage of area correctly identified by the activity image. The disagreement index was defined as:

$$[[N_{act} - N_{both}]/N_{VD}] \times 100\%, \quad \text{Eq. 3}$$

representing the area incorrectly identified by the activity image normalized to the abnormal VD area. The agreement index and the disagreement index were then calculated for the three cutoff thresholds and for three different activity time frames (5–10, 10–20 and 15–30 min after injection) to determine the best overall agreement between ROI_{act} and ROI_{VD}.

Finally, to assess the role of tracer delivery on the difference between VD and FMZ activity images, the asymmetry indices between regions matched and unmatched in the VD and FMZ activity datasets were obtained. This was done for all thresholds separately for VD, FMZ activity and K1 images.

Statistical Analysis

All values are given as mean ± 1 SD. $P < 0.05$ was considered statistically significant. To determine which time frame shows a combination of highest agreement index and lowest disagreement index for all thresholds, we performed a 3 × 3 repeated measures multivariate analysis of variance (ANOVA). After the overall test, posthoc comparisons were performed using a Bonferroni correction for multiple comparisons. A one-way, repeated measures ANOVA was used to determine whether the agreement or the disagreement indices changed significantly with varying threshold. The same test was performed to determine a significant change in the size of the VD abnormality. In addition, a one-way ANOVA was used to show significant differences between the asymmetry indices of VD, K1 and the FMZ activity images. Finally, a 3 × 3 × 2 repeated measures ANOVA was performed to determine multivariate differences between matched and unmatched asymmetry indices derived from VD, K1 and FMZ activity images at the three thresholds.

RESULTS

Normal Asymmetry

The normal mean asymmetry index obtained from VD images in the six healthy subjects was 6.4% ± 1.4%. On the basis of this value, we chose cutoff thresholds of 8% (1.0 SD above mean), 10% (2.5 SD above mean) and 12% (4.0 SD above mean). The FMZ activity images displayed a significantly higher normal mean asymmetry index than the VD images (7.6% ± 1.4%; $P = 0.001$, paired t test).

Size of Image Abnormalities

Figure 1 shows a series of parametric VD and K1 images as well as FMZ activity time frames of 5–10, 10–20 and 15–30 min, obtained from a representative transverse plane in 1 patient. The bottom three rows represent marked images at the 8%, 10% and 12% cutoff thresholds. The size of marked abnormalities in the VD images decreased with increasing cutoff threshold. Furthermore, marked abnormalities in K1 images were always larger than in VD images. The three FMZ activity time frames comprised various contributions from parametric VD and K1 images. It is apparent in Figure 1 that the 5- to 10-min time frame was highly influenced by the K1 image, displaying significantly larger abnormalities than detected in the VD images. The 10- to 20-min FMZ activity time frame showed abnormalities more similar to those found in the parametric VD images when compared with the 15- to 30-min time frame.

The size of abnormal regions obtained from the processed views derived from marked VD images decreased significantly with increasing cutoff threshold (Table 1). At the 10% cutoff threshold, the size of ROI_{VD} was significantly smaller

TABLE 1
Number of Pixels Determined as Abnormal in VD Images (N_{VD}), in 10- to 20-Minute Activity Time Frame (N_{act}) and Common to Both (N_{both}) at 8%, 10% and 12% Cutoff Thresholds

	N_{VD}			N_{act}			N_{both}		
Patient no.	8%	10%	12%	8%	10%	12%	8%	10%	12%
1	387	299	293	751	414	335	308	266	261
2	588	137	0	1192	343	0	385	74	0
3	835	662	325	1081	710	499	730	560	319
4	570	336	288	685	392	302	137	222	191
5	679	430	254	1397	575	357	334	243	194
6	554	180	158	655	239	200	305	170	148
7	1415	933	385	1574	1147	528	1068	707	341

VD = volume of distribution.

than its size at the 8% threshold (56% ± 21%; $P = 0.03$). Furthermore, at the 12% threshold, the size of ROI_{VD} decreased to 37% ± 21% of its size at the 8% threshold ($P = 0.01$).

Dependence of the Agreement Index on the Time Frame

When considering all three asymmetry thresholds, we found a significant difference among the agreement indices obtained from the three activity time frames of 5–10, 10–20 and 15–30 min ($P = 0.03$). The time frame of 10–20 min after FMZ injection proved to have significantly higher agreement with the VD image than the time frames of 5–10 ($P = 0.03$) and 15–30 min ($P = 0.02$) (Fig. 3A). Furthermore, the activity time frame of 10–20 min displayed the lowest disagreement index in all subjects, although this difference was not significant because of the high variance in the data ($P = 0.28$) (Fig. 3B). This result indicates that the time frame of 10–20 min after FMZ injection represents overall the best agreement between activity and VD images independent of the chosen threshold. We therefore chose this activity time frame for all further calculations.

Agreement and Disagreement Indices

The higher normal asymmetry observed in the FMZ activity images compared with the VD images resulted in a large number of false-positive findings at the 8% cutoff threshold, which represents a threshold of only 0.3 SD below normal mean. With the 8% threshold, two of seven patients showed noncontiguous areas of marked abnormalities in the FMZ activity images that were not matched by abnormalities in the VD images (Fig. 1). Table 1 shows the number of pixels determined as abnormal in the VD (N_{VD}) and FMZ activity (N_{act}) images at the 8%, 10% and 12% cutoff thresholds, as well as the number of pixels common to both abnormalities (N_{both}). The agreement and disagreement indices were computed from these values. By increasing the cutoff threshold from 8% to 10%, the agreement index between marked asymmetries in VD and FMZ activity images improved from 62% ± 21% to 75% ± 16% (P = NS) and from 85% ± 12% when the 12% cutoff threshold was used (P = NS). The disagreement index decreased from 92% ± 54% (at the 8% threshold) to 77% ± 68% at the 10% threshold (P = NS) and to 38% ± 16% at the 12% threshold ($P = 0.01$).

Contribution of Tracer Influx

To assess the role of tracer influx on differences between FMZ activity and VD images, the mean asymmetry indices were derived at all three thresholds for VD, FMZ activity and K1 images in those regions in which the marked abnormalities were matched and unmatched. Matched marked abnormalities in VD and FMZ activity images showed similar asymmetry indices in both VD and K1 images for all three thresholds (P = NS, Table 2). Conversely, in those regions that were not matched, the asymmetry indices obtained from VD images were significantly lower than those obtained from FMZ activity images ($P = 0.01$, Table 2). In these regions, the asymmetry indices obtained from K1 images were always higher than the cutoff threshold and were almost identical to those derived from the FMZ activity images (P = NS). This result indicates that differences between the VD and FMZ activity images are mainly caused by the tracer influx parameter K1.

DISCUSSION

The purpose of this study was to determine the agreement between image ROIs obtained from FMZ PET studies using two different protocols: a simplified protocol using images of FMZ activity distribution in only the brain and a protocol that requires collection of arterial blood samples to compute images representing the volume of distribution of the tracer in tissue (VD images). For our analysis, we used abnormalities defined in the parametric VD images as the "gold standard" depicting the seizure focus, to which images obtained using the noninvasive protocol were compared. The VD parameter is currently the most common parameter used for the assessment of epileptic foci with FMZ PET (*6,7*).

The fact that the size of abnormalities in the VD image varies according to the applied cutoff threshold precludes the application of a receiver operator characteristics (ROC)

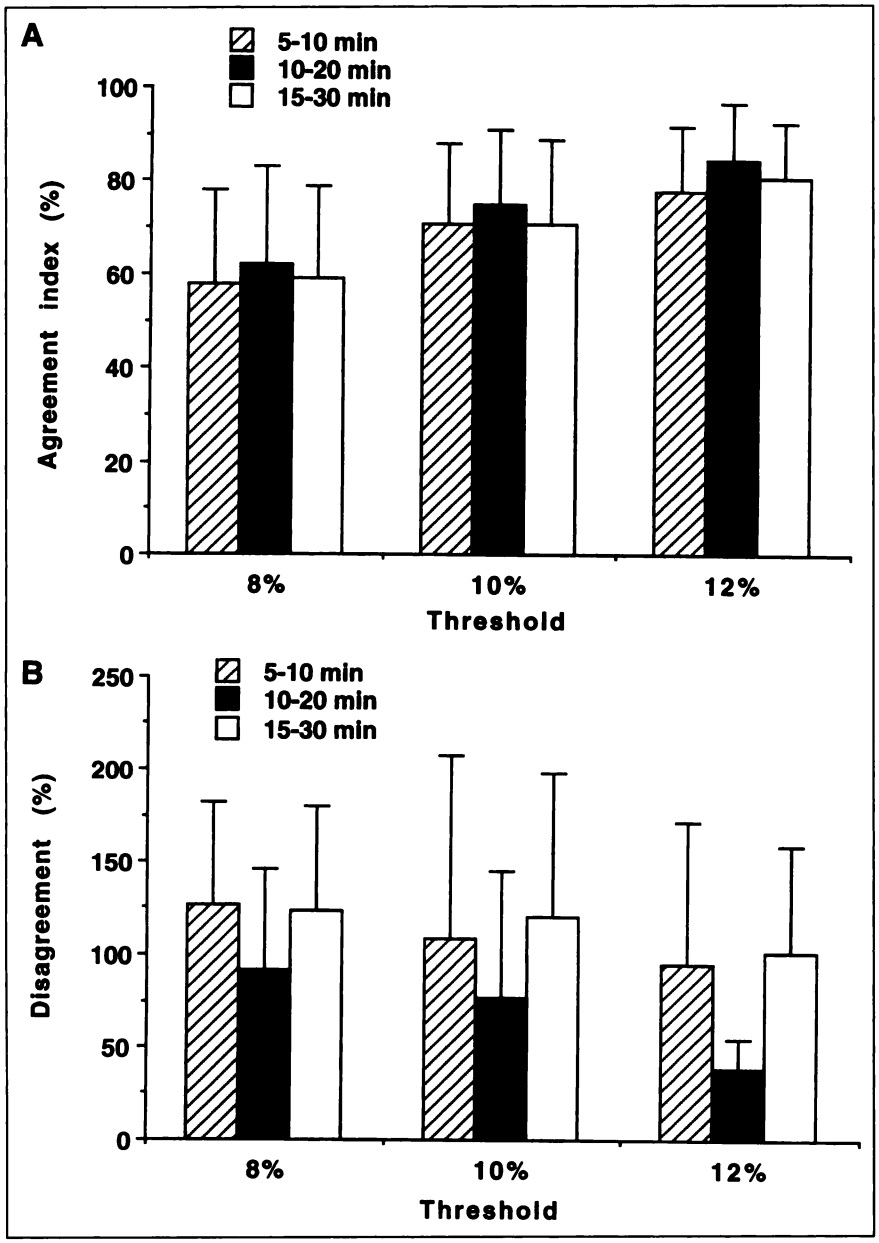

FIGURE 3. (A) Comparison of agreement indices obtained from FMZ activity time frames of 5–10, 10–20 and 15–30 min at 8%, 10% and 12% cutoff thresholds. Agreement index derived from FMZ activity time frame of 10–20 min shows highest agreement index independent of cutoff threshold. (B) Comparison of disagreement indices obtained from FMZ activity time frames of 5–10, 10–20 and 15–30 min at 8%, 10% and 12% cutoff thresholds. FMZ activity time frame of 10–20 min shows lowest disagreement index independent of cutoff threshold.

TABLE 2
Asymmetry Indices Obtained from Matched and Unmatched Defects in VD, FMZ Activity and K1 Images for 8%, 10% and 12% Cutoff Thresholds

	8%		10%		12%	
	Matched	Unmatched	Matched	Unmatched	Matched	Unmatched
VD	11.4	5.1*†	13.9	6.9*†	16.1	8.7*†
SD	2.4	2.0	2.5	2.3	2.6	2.2
FMZ activity	12.7	9.2	14.5	11.0	16.5	13.1
SD	2.6	1.1	2.7	0.6	2.5	1.3
K1	11.9	8.8	13.6	10.8	15.7	13.1
SD	2.0	0.6	2.2	0.6	2.4	0.9

*Significant against unmatched FMZ activity asymmetry threshold ($P < 0.05$).
†Significant against matched VD asymmetry threshold ($P < 0.05$).
VD = volume of distribution; FMZ = [^{11}C]flumazenil; K1 = ligand influx rate constant.

analysis (*14*). To apply an ROC analysis, outcome (in this case the size of abnormality) must be constant and independent of the cutoff threshold. Because of this difficulty, we chose to describe the relationship between ROI_{VD} and ROI_{act} using agreement and disagreement indices. The agreement index is analogous to the sensitivity parameter in the context of an ROC analysis. However, because of the special conditions of our problem, an increase in the cutoff threshold does not decrease agreement (sensitivity) but increases agreement because of changing outcome (size of VD abnormality). To be sensitive to false-positive findings, we defined a disagreement index. Both indices together characterize the extent to which abnormalities in the FMZ activity images approximate VD abnormalities. The data indicate that, by increasing the cutoff threshold, the agreement index steadily increases and the disagreement index decreases. At the same time, however, regions of VD abnormalities decrease in size. As a consequence, there is no optimum, and a compromise must be established between the size of VD abnormalities and the computed agreement and disagreement indices. Our data suggest that the 10% cutoff threshold is a good compromise. The 8% cutoff threshold is too low for FMZ activity, yielding a high incidence of false-positive areas. On the other hand, the 12% cutoff threshold is too restrictive, resulting in a prohibitively small area of VD abnormality.

Our results indicating that FMZ activity images in the time frame of 10–20 min after injection have the highest agreement with VD images confirm a previous report (*12*), which suggested that FMZ activity images around 15 min are qualitatively similar to parametric VD images. At this time frame, the distribution increasingly reflects a pseudo-equilibrium between free and bound ligand; furthermore, peak activity levels are reached in brain between 5 and 15 min after injection. The 5- to 10-min time frames are dominated by tracer influx, whereas the 15- to 30-min images suffer from the short half-life of ^{11}C (20 min) and increasing noise levels caused by tracer efflux.

Earlier studies by Millet et al. (*15*) used FMZ activity images from 20 to 40 min after tracer injection and reported a high correlation between FMZ activity images at this time frame and parametric VD images. However, Millet et al. compared only the performance of the 20- to 40-min time frame with the first 3 min after tracer injection. The results of our study indicate that the time frame of 10–20 min is characterized by a significantly higher agreement with the VD image in identifying regions of asymmetry than the time frame of 5–10 min ($P = 0.03$) and the time frame of 15–30 min ($P = 0.02$).

We hypothesized that differences in tracer influx may account for instances in which there is asymmetry on the FMZ activity images but not on the VD images. Previous PET blood flow studies of focal epilepsy showed a reduction in perfusion (*16–18*) in discrete areas of the brain. However, it was shown previously that the VD parametric image is independent of blood flow (*12,13*). Conversely, the tracer influx image (parametric K1 image) is the product of two factors: cerebral blood flow and blood-brain barrier permeability. It seems unlikely that FMZ transport is affected by alteration at the blood-brain barrier level, because FMZ in blood crosses the blood-brain barrier by passive diffusion caused by its high lipophilicity (*19*). Thus, regionally decreased cerebral blood flow is the main factor responsible for the increased asymmetry in parametric K1 images and is likely to cause the discrepancy observed between FMZ activity and VD images.

Delforge et al. (*20*) have proposed a partial-saturation approach to compute parametric images, allowing the estimation of receptor number and affinity without the necessity of arterial blood sampling. However, this method can be used only under the condition that the patient has a known and constant affinity for BZR. Although this approach does not require an arterial input function, it may not be suitable for epilepsy patients.

CONCLUSION

Abnormalities defined in FMZ activity images obtained from 10 to 20 min after injection using a cutoff threshold of 10% agree well with those obtained from parametric VD images at the same threshold. The noninvasive nature of FMZ activity images makes them very attractive to use for the determination of epileptic foci, particularly in children with partial seizures.

ACKNOWLEDGMENTS

The authors thank Galina Rabkin and Teresa Jones for their expert technical assistance in performing the PET studies. The authors also thank Joel Ager and James Janisse from the Center for Healthcare Effectiveness Research at Wayne State University for their statistical support. This work was partially supported by funding from National Institutes of Health grant NS-34488.

REFERENCES

1. Samson Y, Hantraye P, Baron JC, Soussaline F, Comar D, Maziere M. Kinetics and displacement of [^{11}C]RO 15-1788, a benzodiazepine antagonist, studied in human brain in vivo by positron tomography. *Eur J Pharmacol.* 1985;110:247–251.
2. Persson A, Ehrin E, Eriksson L, et al. Imaging of [^{11}C]-labelled Ro 15-1788 binding to benzodiazepine receptors in the human brain by positron emission tomography. *J Psychiatr Res.* 1985;19:609–622.
3. Shinotoh H, Yamasaki T, Inoue O, et al.Visualization of specific binding sites of benzodiazepine in human brain. *J Nucl Med.* 1986;27:1593–1599.
4. Savic I, Persson A, Roland P, Pauli S, Sedvall G, Widen L. In-vivo demonstration of reduced benzodiazepine receptor binding in human epileptic foci. *Lancet.* 1988;2:863–866.
5. Savic I, Thorell JO, Roland P. [^{11}C]flumazenil positron emission tomography visualizes frontal epileptogenic regions. *Epilepsia.* 1995;36:1225–1232.
6. Henry TR, Frey KA, Sackellares JC, et al. In vivo cerebral metabolism and central benzodiazepine-receptor binding in temporal lobe epilepsy. *Neurology.* 1993;43:1998–2006.
7. Koepp MJ, Richardson MP, Brooks DJ, et al. Cerebral benzo-diazepine receptors in hippocampal sclerosis: an objective in vivo analysis. *Brain.* 1996;119:1677–1687.
8. Szelies B, Weber-Luxenburger G, Pawlik G, et al. MRI-guided flumazenil and FDG-PET in temporal lobe epilepsy. *Neuroimage.* 1996;3:109–118.
9. Koeppe RA, Holthoff VA, Frey KA, Kilbourn MR, Kuhl DE. Compartmental

analysis of [^{11}C]flumazenil kinetics for the estimation of ligand transport rate and receptor distribution using positron emission tomography. *J Cereb Blood Flow Metab.* 1991;11:735–744.
10. Barre L, Debruyne D, Abadie P, Moulin M, Baron JC. A comparison of methods for the separation of [^{11}C]Ro 15-1788 (flumazenil) from its metabolites in the blood of rabbits, baboons and humans. *Int J Rad Appl Instrum.* 1991;42:435–439.
11. Muzik O, Chugani DC, Shen C, et al. Objective method for localization of cortical asymmetries using positron emission tomography to aid surgical resection of epileptic foci. *Comput Aided Surg.* 1998;3:74–82.
12. Frey KA, Holthoff VA, Koeppe RA, Jewett DM, Kilbourn MR, Kuhl DE. Parametric in vivo imaging of benzo-diazepine receptor distribution in human brain. *Ann Neurol.* 1991;30:663–672.
13. Holthoff VA, Koeppe RA, Frey KA, Paradise AH, Kuhl DE. Differentiation of radioligand delivery and binding in the brain: validation of a two-compartment model for [^{11}C]flumazenil. *J Cereb Blood Flow Metab.* 1991;11:745–752.
14. Metz C. Basic principles of ROC analysis. *Semin Nucl Med.* 1978;8:283–298.
15. Millet P, Delforge J, Mauguiere F, et al. Parameter and index images of benzodiazepine receptor concentration in the brain. *J Nucl Med.* 1995;36:1462–1471.
16. Bernardi S, Trimble MR, Frackowiak RS, Wise RJ, Jones T. An interictal study of partial epilepsy using positron emission tomography and the oxygen-15 inhalation technique. *J Neurol Neurosurg Psychiatry.* 1983;46:473–477.
17. Kuhl DE, Engel J Jr, Phelps ME, Selin C. Epileptic patterns of local cerebral metabolism and perfusion in humans determined by emission computed tomography of ^{18}FDG and ^{13}NH3. *Ann Neurol.* 1980;8:348–360.
18. Lee BI, Markand ON, Wellman HN, et al. HIPDM-SPECT in patients with medically intractable complex partial seizures: ictal study. *Arch Neurol.* 1988;45:397–402.
19. Roncari G, Ziegler W, Guentert T. Pharmacokinetics of the new benzodiazepine antagonist Ro 15-1788 in man following intravenous and oral administration. *Br J Clin Pharmacol.* 1986;22:421–428.
20. Delforge J, Spelle L, Bendriem B, Samson Y, Syrota A. Parametric images of benzodiazepine receptor concentration using a partial-saturation injection. *J Cereb Blood Flow Metab.* 1997;17:343–355.